치의과학박사학위논문

Chemical Properties and Biocompatibility of Nanohybrid Dental Composites

치과용 나노하이브리드 복합레진의 화학적 특성과 생체적합성에 관한 연구

2023 년 2 월

서울대학교 대학원

치의과학과 치과생체재료과학

JIANG ENSHI

Chemical Properties and Biocompatibility of Nanohybrid Dental Composites

지도교수 정 신 혜

이 논문을 치의과학박사학위논문으로 제출함

2022 년 11 월

서울대학교 대학원

치의과학과 치과생체재료과학전공

JIANG ENSHI

JIANG ENSHI 의 치의과학박사학위논문을 인준함

2023 년 1 월

위 원 장 임 범 순 (인)

부 위 원 장 정 신 혜 (인)

위 원 이 상 훈 (인)

위 원 장 주 혜 (인)

위 원 오 소 람 (인)

Abstract

Chemical Properties and Biocompatibility of Nanohybrid Dental Composites

JIANG ENSHI, D.D.S.

Department of Dental Biomaterials Science,

School of Dentistry, Seoul National University

Objective

This study aimed to investigate the basic characteristics of nanohybrid composites by assessing the filler particle size distribution, degree of conversion (DC), and translucency parameters (TP). And investigated the chemical and biological characteristics of three nanohybrid composites by evaluating the monomer content of the composite eluates, the cell response to the composite eluates via cell cytotoxicity test, real-time intracellular reactive oxygen species (ROS) generation, and cell proliferation test.

Materials and methods

Three nanohybrid composite resins (TN, Tetric N-Ceram; CX, Ceram X Sphere Tec One; and DN, DenFil NX) were used, and the size distribution of the filler particles was analyzed using scanning electron microscopy (SEM) followed by image

analysis (n = 5). After light-polymerization for 20 s and 40 s, the DC was measured via micro-Raman spectroscopy (n = 3). TP values of the three composites were measured before and after thermocycling 10,000 times (n = 5). The components of polymerized composites were evaluated by gas chromatography/mass spectrometry (GC/MS; n = 3). Dulbecco's modified Eagle's medium (DMEM), the cell culture medium for the human gingival fibroblast cell line (HGF-1), was used to elute composites for 24 h. Water-soluble tetrazolium-1 (WST-1) assay (n = 9), trypan blue exclusion test (n = 9), and live/dead assay (n = 9) were performed to determine the cytotoxicity. Real-time intracellular ROS generation (n = 9) was measured by a cell imaging multi-mode reader. In addition, the cell proliferation test was performed for 7 days. The statistical significance of the differences among composites was assessed using an analysis of variance, followed by Bonferroni multiple comparison tests (α = 0.05).

Results

Morphological variations in the different-sized fillers were observed in the composites, and the distribution of the nanofiller contents was similar in CX and DN**.** The DC values did not significantly differ between composites but were significantly different between 40 s and 20 s polymerization time ($p < 0.05$). There were no significant differences in TP values among the composite before and after aging ($p > 0.05$). Different compositions of monomers and additives were detected in the three composites using GC/MS, the amounts of triethylene glycol dimethacrylate (TEGDMA) in CX were higher than those in others ($p < 0.0001$). 2-hydroxyethyl methacrylate (HEMA) was not detected in CX, while higher in TN than in DN ($p = 0.0015$). BPA was not detected in any composites. The lowest cell viability was observed for CX and the highest cell viability was detected in DN ($p <$

0.0001). The highest ROS formation was detected in TN, followed by CX and DN ($p < 0.0001$) at 8 h, 12 h, and 16 h. The lowest relative cell survival was recorded in CX ($p < 0.0001$), while there was no significant difference in DN and TN compared with NC ($p > 0.05$) on day 7.

Conclusion

The three nanohybrid dental composites exhibited various compositions of filler sizes and resin components, resulting in different levels of cytotoxicity, ROS production, and cell survival. CX showed the highest cytotoxicity induced by ROS accumulation followed by TN. DN presented no significant ROS accumulation and showed the highest cell viability for 7 days.

Keywords: Nanohybrid, Composite resin, Gas chromatography/mass spectrometry, Cytocompatibility, Relative oxygen species

***Student Number*:** 2020-31168

Table of Contents

Tables and Figures

1. Introduction

1.1 Background

Wide-ranging applications of resin-based composites in restorative dentistry have facilitated the improvement of mechanical and aesthetic features as well as clinical performance. Various technologies have been introduced to enhance the material properties, mainly those dealing with changes in filler components and monomer-matrix formulation. Among restorative composite resins with various filler distributions, nanohybrid composites incorporate both nano-ranged sizes of fillers (0.005 – 0.01 μm) and microsized fillers (0.01 – 0.04 μm) [5]. The nanosized fillers are smaller than the visible light wavelengths and occupy larger spaces between particles [6]. Additional filler loading by submicron-sized particles led to improved surface qualities, such as superior polishing and gloss retention, compared to conventional micro-hybrid composites [7, 8]. However, small sizes of filler particles increase the surface area-to-volume ratios of the fillers, which may render the polymerized structures prone to water uptake and induce interfacial degradation of the resin matrix and filler particles [8]. In addition, water absorption and moisture permeation into the pores within an incompletely polymerized resin matrix can induce the leaching of unreacted monomers, unbound substances, and water-soluble elements [9, 10].

Studies have raised clinical safety concerns regarding the leaching of monomers and additives released from resin-based composites into the oral environment under diverse polymerizing conditions [11-13]. Cell death caused by deoxyribonucleic acid (DNA) double-strand breakage, alveolar bone resorption by increased inflammatory

cytokine activity, an inflammatory reaction due to increased cyclooxygenase-2 (COX-2) enzyme, and acute systemic toxicity is significant concerns for the leaching of components [13-16]. Bisphenol-A (BPA) is a well-known endocrine disruptor that can be present as an impurity or degradation product of BPA-based monomers [17]. Co-monomers with low molecular weights, such as triethylene glycol dimethacrylate (TEGDMA) and 2-hydroxyethyl methacrylate (HEMA), are more mobile and absorbent, and readily leach into the immersion medium relative to basic monomers with high molecular weights, such as bisphenol A glycidyl methacrylate (Bis-GMA), bisphenol A ethoxylated dimethacrylate (Bis-EMA), and urethane dimethacrylate (UDMA) [11]. Exposure to TEGDMA, HEMA, or UDMA can produce reactive oxygen species (ROS) leading to cell damage [18, 19]. Further, the elevated exposure levels can detrimentally induce DNA damage and cell death [20-22].

Considering the large variety of compositions of light-polymerized composite resins and their diverse usage in restorative dentistry, the potential risks of resin components leaching out into the oral cavity can be a significant concern for patients and practitioners. Therefore, it is essential that the biocompatibility of polymerized resins is assessed at the level of individual eluates, quantitatively and qualitatively. Gas chromatography/mass spectrometry (GC/MS) has been used to identify additives, smaller monomers, co-monomers, other volatile compounds, and decomposition and fragmentation products [23]. A strong correlation between the number of eluates and cell viability has been observed using various cell lines and different test methods [21, 24-28]. Further, components released from polymerized resins can affect cellular signaling networks by generating ROS, in the same pattern detected with cytotoxic effects [25]. Moreover, the cross-linking structures of the matrix monomers and dispersed inorganic fillers can mutually impact the

reachability of unbound monomers; thus, the filler content is an interesting topic for investigating the toxicity of composite materials.

Differences in the resin matrix and filler composition in nanohybrid composites (Tetric N-Ceram, TN; Ceram X Sphere Tec One, CX; and DenFil NX, DN) are summarized in Table 1. TN and DN equally contained monomers of UDMA and BPA-based monomers, while CX contained only UDMA. TEGDMA, a dilute monomer, equally contained all of them. TN, CX, and DN equally contained inorganic elements of barium (Ba) and silicon (Si), while CX additionally contained fluorine (F). However, limited information is available to dental practitioners when selecting the material considering safety issues in relation to leaching components of nanohybrid composites.

1.2 Purpose of Research

This study aimed to compare the biological properties of three nanohybrid dental composites by assessing the cytotoxicity and ROS production of the composite eluates. The monomer composition, DC, and nanofiller content of the composites were determined using GC/MS, micro-Raman spectroscopy, and scanning electron microscopy (SEM).

The null hypothesis was that the components eluted from the three commercials nanohybrid dental composites would show no differences in nanofiller content, DC, TP, cytotoxicity, ROS production, and relative cell survival.

2. Materials and Methods

Three commercial nanohybrid resin-based composites (TN, CX, and DN) were used in this study. The experiment flow diagram is shown in Figure 1.

2.1 Specimen preparation

The filler particle preparation process is shown in Figure 2. To retain the inorganic fillers the organic components of the composites were dissolved before polymerization. Each resin (300 mg) was placed in 10 mL amber glass vials (SciLab, Daegu, Korea). To the vials, 6 mL of acetone (99.5%, Sigma-Aldrich, Saint Louis, MO, US), chloroform (99.8% HPLC grade, Sigma-Aldrich), and absolute ethanol (Sigma-Aldrich) were added successively and maintained for 24 h at room temperature each. During the holding time, samples were centrifuged at 1,200 rpm for 6 min three times. The supernatants were discarded, and the remaining precipitate in the glass vial was placed on a hot plate (PC-420D, Corning, New York, NY, USA) and dried overnight (12 h) at 37 °C.

The specimen preparation process is shown in Figure 3. For light polymerization, the resin was shaped into disk-shaped specimens in a Teflon mold (13 mm diameter and 1 mm thickness). Both the top and bottom surfaces were divided into four areas and polymerized for 20 s and 40 s using a 9 mm diameter light-emitting diode (LED) curing unit (Elipar DeepCure-S LED Curing Light, 3M ESPE, Seefeld, Germany) with a wavelength of 430 – 480 nm and a light intensity of 850 – 950 mW/cm^2 controlled by a radiometer (Demetron LED Radiometer, Kerr Sybron Dental Specialties, Middleton, WI, USA). To simulate the clinical situation of an occlusal composite restoration, the top outer surface was not covered with a

Mylar strip to mimic the oxygen-inhibited layer, whereas the bottom surface was covered with a glass slide. Specimens with and without polymerization were immediately used to measure the DC.

After light-polymerization for 40 s, specimen aging simulated at 5 ℃ and 55 ℃ for 10,000 cycles using a thermocycler (THE1200, SD Mechatronik, Feldkirchen Westerham, Bavaria, Germany). Specimens before and after simulated aging were used to measure the TP.

The experimental process of the composite eluates is shown in Figure 4. To prepare the composites eluate for chemical evaluation (Figure 4A), three composite specimens (n = 3), which were light-polymerized for 40 s, in an amber glass vial (SciLab), were eluted with methanol (HPLC grade 99.9%, Sigma-Aldrich), (3 cm^2/mL) for 24 h at 37 °C. They were then filtered using a membrane filter unit (0.45 μm, Corning), and 1 mL of the filtrate was used for GC/MS analysis.

To prepare the composite eluates for biological tests (WST–1, live/dead, ROS generation, and cell proliferation assays), the samples (3 cm^2/mL as defined in ISO 10993–5:2009) were immersed in Dulbecco's modified Eagle medium (DMEM, Hyclone, Logan, UT, USA) for 24 h at 37 ℃ in ~~the~~ dark, after polymerization for 40 s. Samples were then filtered using a membrane filter unit (0.22 μm, Corning). Composite eluates at 100% concentration were used for the following biological analysis.

2.2 Characteristics of filler particles

Morphological analysis of the filler particles was performed by SEM (Apreo S, Thermo Scientific, Waltham, MA, USA). Samples were fixed to the sputter-coated carbon stubs and sputter-coated with platinum using a turbomolecular pumped coater

(Q150T S, Quorum Technologies, Sacramento, California, USA) with 20 mA sputter current at a 2.3 tooling factor for 360 s. SEM images were recorded at magnifications of 1,000×, 5,000×, and 30,000× (10 kV, 0.1 nA; working distance of 10 mm, n = 5). The size distribution of filler particles smaller than 1 μm was determined using the SEM of 1,000 random particles at a magnification of 30,000× (n = 5). The distribution of spherical filler particles larger than 1 μm was determined using SEM of 100 random particles (n = 5). ImageJ (ver. 1.53, National Institutes of Health, Bethesda, MD, USA) was used to count and measure the size of the filler particles [29, 30].

2.3 DC assessment

Five points of each specimen (n = 3) were evaluated with a 532 nm laser-equipped, micro-Raman microscope (DXR2xi, Thermo), with a spectral resolution of approximately 5 cm^{-1} and a spectral range of 2000 – 1000 cm^{-1}. A 50× objective lens was used to obtain the spectra. During polymerization, the peak intensity decreased with the conversion of the aliphatic double-carbon structure to form polymer chains. The following equation was used to calculate the DC:

$$\text{DC}\ (\%) = 1 - \frac{R_{Polymerized}}{R_{Unpolymerized}} \times 100$$

where R is the ratio of the peak intensities at 1639 cm^{-1} and 1609 cm^{-1} associated with the aliphatic and aromatic stretching in the nanohybrid composites, respectively.

2.4 TP measurement

A spectrophotometer was used to determine the International Commission on Illumination L*a*b* (CIELAB) and the TP was calculated (Color i7, X-Rite, Grand Rapids, MI, USA). The D65-10 optical configuration was used, with a 3 mm aperture. The means of three measurements were recorded for each specimen. The mean L*,

a*, and b* values for the white and black backgrounds used for the TP calculations were 95.92 and 0.04, respectively. TP values were calculated by subtracting the measurements against black and white backgrounds using the following formula.

$$\mathrm{TP} = [(L_W^* - L_B^*)^2 + (a_W^* - a_B^*)^2 + (b_W^* - b_B^*)^2]^{\frac{1}{2}}$$

2.5 GC/MS analysis of composite eluates

The eluted components were evaluated both qualitatively and quantitatively, and the additives were analyzed qualitatively. A Trace Ultra GC Ultra gas chromatograph linked to a triple quadrupole mass spectrometer (TSQ 8000, Thermo Fisher Scientific) was used and transfused in the splitless mode. The compounds were separated using a GC column with geometry parameters of 60 m in length, 0.25 mm in diameter, and 0.25 μm in film thickness at a stationary phase with a split ratio of 1:10 and helium flowing at a constant rate of 1 mL/min. The GC oven was heated isothermally at 50 ℃ for 2 min, heated to 280 ℃ (25 ℃/min), held for 5 min, and then cooled to 250 °C. With an electron ionization (EI) source temperature of 240 ℃, the mass spectrometer (MS) was set to the full scan mode, and data were recorded (50 – 600 m/z) at 70 eV. For qualitative analysis, the relevant compounds were identified by comparing their retention times and mass spectra with their corresponding reference standards and the National Institute of Standards and Technology (NIST) library database [31]. Calibration was performed for each standard compound for the quantitative analysis of TEGDMA, HEMA, and BPA. The limit of quantification (LOQ) was in the range of 0.1 – 1,000 μg/mL.

2.6 Cell culture

The human gingival fibroblast cell line (HGF-1, ATCC CRL-2014) was cultured in DMEM containing 1% penicillin (Gibco, Life Technologies, Grand Island, NY,

USA), 1% streptomycin (Gibco), and 10% fetal bovine serum (FBS, Gibco) at 37 ℃ in a humidified chamber with 5% CO_2. The cells were seeded in a 100 mm culture dish (SPL Life Sciences, Yeoju-si, Gyeonggi-do, Korea) and evaluated after the cells reaching 80% confluency.

2.7 Cell cytotoxicity test

2.7.1 WST-1 assay

HGF-1 cells were seeded in a 24 well plate (SPL) at a concentration of 2×10^4 cells/mL and incubated for 24 h. Then, the cells were exposed with 1 mL of 100% composite eluates and incubated for another 24 h. The negative control (NC) group was treated with DMEM alone without eluates. For the WST-1 assay, the EZ–Cytox cell viability assay kit (DoGen Bio, Seoul, Korea) was used to determine cell cytotoxicity. WST-1 regent in DMEM (1:10) was treated to cells for 3 h at 37 ℃. Optical density (OD) was determined at 450 nm using a microplate reader (AMR-100, Allsheng, Hangzhou, Zhejiang, China). The relative cell viability was calculated as the ratio of the OD of the experimental groups (TN, CX, and DN) to that of the NC. The experiments were performed in triplicate (n = 9).

2.7.2 Trypan blue exclusion test

Cells were seeded in a 24 well plate (SPL) at a concentration of 2×10^4 cells/mL and incubated for 24 h. After that, cells were treated with 1 mL of 100% composite eluate and incubated for 24 h. The NC group was treated with DMEM alone. Cells were harvested using trypsin (0.25%, Hyclone) and resuspended. Cells were stained by trypan blue (0.4%, Gibco) and counted using a cell counting chip (C Chip, Cheonan-si, Chungchengnam-do, Korea). The experiments were performed three times (n = 9).

2.7.3 Live/dead assay

Cells were seeded in a 35 mm confocal dish (SPL) at a concentration of 2×10^4 cells/mL and incubated for 24 h. Cells were exposed to 1 mL of 100% composite eluates and incubated for another 24 h. The NC group was treated with DMEM alone without eluates, and the positive control (PC) group was treated with 1 mM H_2O_2 (Sigma-Aldrich). Viable and dead cells were observed via the live/dead assay (LIVE/DEAD Viability kit, Invitrogen, Waltham, MA, USA) under a digital inverted fluorescence microscope (DS-Ri2, Nikon Corporation, Tokyo, Japan) and a confocal laser microscope (LSM 700, Carl Zeiss, Thornwood, NY, USA). Live cells were observed with green fluorescence, and dead cells were observed with bright red fluorescence.

2.8 Generation of intercellular ROS

HGF-1 cells were seeded in the wells of black, flat-bottom 96 well plates (Greiner Bio-One, Frickenhause, Germany) at a density of 1×10^4 cells/mL and incubated for 24 h. After incubation, the medium was changed to 100 μL of the 100% composite extracts containing 5 μM CellROX Green Reagent (Invitrogen; Life Technologies, Carlsbad, CA, USA) and incubated at 37 °C. Upon oxidation, the CellROX green reagent binds to DNA, and its signal is primarily localized in both the nucleus and mitochondria. Green fluorescence was detected when the reagent was oxidized by ROS and then bound to DNA. To confirm the intracellular reaction, images and fluorescence intensities were recorded every 15 min for 16 h using a multi-mode plate reader (Cytation 7, BioTek, Winooski, VT, USA). The percentages of fluorescence intensities and ROS production areas were analyzed using data analysis

software (ver. 1.9, Gen5, Biotek). The experiments were performed in triplicate (n = 9).

2.9 Cell proliferation test

Cells were seeded in a 24 well plate (SPL) at a concentration of 2×10^4 cells/mL and incubated for 24 h. Cells were stimulated by 1 mL 100% composite eluate for 7 days. The medium was changed every 3 days. The NC group was treated with DMEM alone without composites eluate. The PC group was treated with 1 mM H_2O_2 (Sigma-Aldrich). For WST-1 assay, the EZ–Cytox cell viability assay kit (DoGen Bio) was used. WST-1 reagent was added in a concentration of 10% in DMEM. Cells were incubated for another 3 h at 37 ℃ 5% CO_2. The OD was determined at 450 nm using a microplate reader (Allsheng). Relative cell survival was calculated as the ratio of the OD of the experimental groups (TN, CX, and DN) to that of the NC on day 1. The experiments were repeated three times (n = 9).

2.10 Statistical analysis

The data were averaged from three replicates. All data are presented as the mean and standard deviation. Software GraphPad Prism (ver.9.0.0., San Diego, CA, USA) was used for statistical analyses. The significance of the differences between the groups was determined using a one-way analysis of variance with the Bonferroni multiple comparison test. Statistical significance was set at $p < 0.05$.

3. Results

3.1 Characteristics of filler particles

All composite materials showed morphological variations of differently-sized fillers in SEM images (Figure 5). Filler particles smaller than 0.1 μm comprised 26.09%, 27.00%, and 7.63% of the total distribution in CX, DN, and TN, respectively (Figure 6). TN exhibited submicron-sized fillers mixed with a shape of irregular or spherical particles (the mean size = 0.13 ± 0.02 μm). In CX and DN, larger spherical particles (12.87 ± 6.08 μm and 8.98 ± 4.11 μm, respectively) were mixed with irregularly shaped fillers of submicron size.

3.2 DC measurement

The micro-Raman spectra obtained immediately before and after light polymerization are presented in Figure 3. The peak intensities of 1609 cm^{-1} at 1639 cm^{-1} were associated with C=C aliphatic and aromatic stretching bonds in the polymeric matrix, respectively. The DC values of 40 s light-polymerized TN (70.61 ± 4.27%), CX (69.13 ± 4.46%), and DN (72.06 ± 3.72%) were not significantly different ($p > 0.05$; Figure 7). The DC values of 20 s light-polymerized TN (64.05 ± 2.42 %), CX (63.40 ± 2.46%), and DN (65.45 ± 3.35%) did not significantly differ ($p > 0.05$). DC of 40 s light polymerized in three groups (TN, CX, and DN) was significantly higher than that of 20 s light-polymerized groups ($p = 0.0118$, $p = 0.0426$, and $p = 0.0109$, respectively).

3.3 TP measurement

Table 2 presents the CIELAB values of the tested composites. The L*, a*, and b* values of white and black were not significantly different before and after simulated

ging among the three composites ($p > 0.05$). Figure 8 shows no significant difference in TP values among the three composites before and after aging ($p > 0.05$).

3.4 GC/MS analysis of composite eluate

Representative GC/MS chromatograms of the individual substances in TN, CX, and DN are shown in Figure 9. HEMA was detected in both TN and DN, while TEGDMA was observed in all composites. The photoinitiator, camphorquinone (CQ), and the co-initiator, 4-dimethylaminobenzoic acid ethyl ester (DMABEE), were detected in all the composites. The detected components of the co-monomers and other additives are listed in Table 3. The standard components used in this study are listed in Table 4. The GC/MS chromatograms of the standards are shown in Figure 10. The calibration curves are shown in Figure 11. The amounts of HEMA were 259.46 ± 53.14 μg/mL (1.99 mM) in TN, 43.91 ± 3.32 μg/mL (0.34 mM) in DN, and not detected in CX (Table 4 and Figure 12). The amount of TEGDMA (1,081.10 ± 128.61 μg/mL, 3.7 mM) in CX was higher than those in TN (23.3 ± 0.06 μg/mL, 0.08 mM) and DN (38.80 ± 3.50 μg/mL. 0.13 mM) ($p < 0.0001$). BPA was not detected in any of the composites.

3.5 Cell cytotoxicity test

3.5.1 WST-1 assay

The relative cell viability was lowest in CX (61.25 ± 3.1%), followed by TN (82.10 ± 3.8%) and DN (100.7 ± 6.4%; Figure 13, $p < 0.0001$). There was no significant difference between DN and NC ($p > 0.05$).

3.5.2 Trypan blue exclusion test

The cell number was highest in DN; there was no significant difference compared with NC. The cell number of TN and CX was significantly lower than that in NC (Figure 14; $p < 0.0001$).

3.5.3 Live/dead assay

Representative fluorescent staining images of HGF-1 cells after treatment with each composite eluates for 24 h are presented in Figure 15. PC showed the dead fluorescent red cells. NC, TN, and DN showed similar patterns of fluorescent green cells, while CX showed a dissimilar cell morphology that was less homogeneous with shrunken cellular processes.

3.6 Generation of intercellular ROS

The fluorescent digital image correlation (DIC) micrograph profiles showed ROS generation every 4 h (Figure 16). The relative average intensity and sum area of green fluorescence significantly increased in TN and CX at 8, 12, and 16 h compared to that in NC and DN (Figures 17 and 18, $p < 0.0001$) There was no significant difference between DN and NC for 16 h ($p > 0.05$).

3.7 Cell proliferation test

The OD of CX presented a decreasing trend, while TN and DN showed an increasing trend during 7 days (Figure 19). At day 3, the relative cell survival of CX was decreased and there was no significant difference compared with PC ($p > 0.05$). The relative cell survival of TN and DN was increased and higher than NC (Figure 20, $p < 0.0001$). At day 7, there was no significant difference in TN and DN compared with NC ($p > 0.05$). CX was still the lowest group compared with NC, TN, and DN ($p < 0.0001$).

4. Discussion

Based on the results, there was no significant difference in TP and DC among the three composites. The three nanohybrid composite eluates exhibited different monomers and additives compositions. HEMA and TEGDMA, representative co-monomers with low molecular weights and high mobility, were eluted in different amounts in the three composites, affecting the cell viability and ROS production to dissimilar levels. Therefore, the null hypothesis was rejected.

Currently, the available nanohybrid composite resins enhance filler loading and also replace conventional monomer-matrix formulations to maintain adequate consistency and aesthetic properties. It is common for manufacturers to indicate only the total volume and weight of the filler contents. Additionally, the remaining volume is occupied by resin matrix monomers and other trace additives that users are unaware of. This study focused on co-monomers of low molecular weight, which increased the polymerizing effectiveness and calibrated efficiency, rather than the backbone monomers of high molecular weight with elevated mechanical and chemical stabilities. The intensity of cytotoxicity of the monomers released from restorative composites, the intensity of cytotoxicity of monomers was ranked as Bis-GMA > UDMA > TEGDMA > HEMA [32, 33]. However, the order of the releasing tendency is known to be HEMA > TEGDMA > UDMA > Bis-GMA, indicating the elution capacity of small-sized monomers [11]. For methacrylate cross-linking monomers, differences exist in the magnitude of the released quantities between organic solvents and water-based solutions [28]. The GC/MS experimental method is based on the vaporization and ionization of ingredients of low molecular weight

compounds. Methanol was chosen to meet the LOQ owing to its high dissolution efficiency. In our results, CX showed the highest TEGDMA level, the lowest cell viability, and a time-dependent increase in ROS production. For HEMA, the value detected in TN (1.9 mM) was higher than that in DN (0.34 mM) and CX (not detectable). It has been widely reported that HEMA could be a degradation product of urethane dimethacrylate (UDMA) as a basic monomer with a high molecular weight [34]. UDMA is also a basic component in the TN, as claimed by the manufacturer, and the higher concentration of HEMA detected in TN was regarded to be derived from UDMA. In our GC/MS, a standard UDMA (≥ 97%, Sigma-Aldrich, Cat no. 72869-86-4) was analyzed, and the peaks were confirmed as four single peaks and one single peak of HEMA. In a previous study involving monomer release from dentin bonding systems, when methanol was used to extract the resin components, the mean content of HEMA in methanol was 10 times higher than that in distilled water [35]. Upon oxidation, the cell ROX green reagent binds to DNA; thus, its signal is primarily localized in the nucleus and mitochondria. The half maximal effective concentration (EC_{50}) values of HEMA for the viability of HGFs were 11.2 mM and the concentration inducing DNA strand breakdown was 1.12 mM [36]. Despite being extracted in methanol, HEMA was prominently detected in the TN group and might have affected ROS generation. Conventionally, BPA is a component that has been at the center of debate owing to its xenoestrogenic potential, resulting in systemic consequences. However, many previous studies that applied highly sensitive analytical methods did not reveal the presence of BPA as an impurity during manufacturing. Biodegradation of BPA-based basic monomers into BPA is also feasible under the extremes of the oral environment, such as pH fluctuations, enzymatic degradation, as well as thermal and mechanical challenges. However,

only trace amounts could be detected under hazardous limits, particularly with the experimental settings for short-term elution [17]. We did not detect BPA in the eluates from the three composites, even when methanol was used as an immersion medium to dissolve extractable compounds.

In our study, the level of DC reached approximately 70%, without significant differences among composites. Therefore, differences in the release of unpolymerized monomers did not seem to result from the different degrees of polymerization of the composites. Interestingly, no significant cytotoxicity or ROS generation was observed in the DN group compared with NC. Apart from the relatively low elution of TEGDMA and HEMA in DN, the volumetric content of fillers was higher in DN than in others (Table 1). We assumed that the lower content of matrix monomer in DN might contribute to the smaller amount of monomer released, resulting in better biocompatibility. Another point to consider regarding the relatively lower level of cytotoxicity detected in DN is that DN does not contain any fluoride compounds that are claimed to be the contents of TN and CX. Even novel composites containing synthetic fillers conjugated with fluoride ions have significant levels of anti-cariogenic potential, but no detectable level of cytotoxicity [37, 38]. However, it will be meaningful to investigate the ionic release capacity of the composites in addition to their monomer elution.

Regarding our limited experimental design, it is difficult to extrapolate the results to clinical circumstances. As restorative composite resins are composed of various compounds, no single detection method can help evaluate every compound with various molecular weights and chemical formulas. Nonetheless, comprehensive chemical analyses are warrented to evaluate monomers of higher molecular weight, such as Bis-GMA and UDMA [39]. In addition, the selection of the immersion

medium is a complicated issue. Even when human saliva is used, thermal, chemical, and bacterial conditions must be incorporated to assimilate *in vivo* conditions [40]. A constant exchange of the immersion medium must also be considered to simulate salivary flushing in the mouth. In addition, mechanical impacts on restorative surfaces during intraoral service of dental composites should be considered, as dislodgement of surface fillers from the matrix can be developed, accelerating monomer elution [41]. Future studies should investigate more clinically relevant conditions and reflect these factors in experimental settings.

5. Conclusion

Based on this study, three nanohybrid dental composites exhibited various compositions of filler sizes and resin components, resulting in different levels of cytotoxicity and ROS production. Chemical compositions of dental composites can be considered with their biological impact on safety issues in the intraoral use of dental restorative composites. The composites eluate (CX) with the highest TEGDMA showed the highest cytotoxicity induced by ROS accumulation. The composites eluate (DN) contained the lower TEGDMA and HEMA presented the highest cell viability.

References

1. Van Dijken J, Pallesen U. A randomized 10-year prospective follow-up of Class II nanohybrid and conventional hybrid resin composite restorations. J Adhes Dent. 2014;16:585-92.
2. Alzraikat H, Burrow M, Maghaireh G, Taha N. Nanofilled resin composite properties and clinical performance: a review. Oper Dent. 2018;43:E173-90.
3. Durner J, Obermaier J, Draenert M, Ilie N. Correlation of the degree of conversion with the amount of elutable substances in nano-hybrid dental composites. Dent Mater. 2012;28:1146-53.
4. Yadav R, Meena A, Patnaik A. Biomaterials for dental composite applications: A comprehensive review of physical, chemical, mechanical, thermal, tribological, and biological properties. Polym Adv Technol. 2022; 33:1762-81.
5. Bastos NA, Bitencourt SB, Martins EA, De Souza GM. Review of nano-technology applications in resin-based restorative materials. J Esthet Dent. 2021;33:567-82.
6. Heintze S, Forjanic M, Ohmiti K, Rousson V. Surface deterioration of dental materials after simulated toothbrushing in relation to brushing time and load. Dent Mater. 2010;26:306-19.
7. Kaizer MR, de Oliveira-Ogliari A, Cenci MS, Opdam NJ, Moraes RR. Do nanofill or submicron composites show improved smoothness and gloss? A systematic review of in vitro studies. Dent Mater. 2014;30:e41-78.
8. Maran BM, de Geus JL, Gutiérrez MF, Heintze S, Tardem C, Barceleiro MO, Reis A, Loguercio AD. Nanofilled/nanohybrid and hybrid resin-based

composite in patients with direct restorations in posterior teeth: A systematic review and meta-analysis. J Dent. 2020;99:103407.

9. Nasution H, Tantra A, Arista T. The effect of filler content and particle size on the impact strength and water absorption of epoxy/cockle-shell powder (Anadora granosa) composite. ARPN J Eng Appl Sci. 2016;11:4739-42.

10. Örtengren U, Wellendorf H, Karlsson S, Ruyter I. Water sorption and solubility of dental composites and identification of monomers released in an aqueous environment. J Oral Rehabil. 2001;28:1106-15.

11. Van Landuyt K, Nawrot T, Geebelen B, De Munck J, Snauwaert J, Yoshihara K, Scheers H, Godderis L, Hoet P, Van Meerbeek B. How much do resin-based dental materials release? A meta-analytical approach. Dent Mater. 2011;27:723-47.

12. Bationo R, Rouamba A, Diarra A, Beugré-Kouassi MLA, Beugré JB, Jordana F. Cytotoxicity evaluation of dental and orthodontic light-cured composite resins. Clin Exp Dent Res. 2021;7:40-8.

13. Yang Y, Reichl FX, Shi J, He X, Hickel R, Högg C. Cytotoxicity and DNA double-strand breaks in human gingival fibroblasts exposed to eluates of dental composites. Dent Mater. 2018;34:201-8.

14. Urcan E, Scherthan H, Styllou M, Haertel U, Hickel R, Reichl FX. Induction of DNA double-strand breaks in primary gingival fibroblasts by exposure to dental resin composites. Biomaterials. 2010; 31:2010-4.

15. Schmalz G. Determination of biocompatibility: evaluation of materials. In: Schmalz G, Arenholt D editors. Biocompatibility of dental materials. Leipzig, Springer; 2009: p. 13-43.

16. Peskersoy C, Oguzhan A, Gurlek O. The Effect of Flowable Composite Resins on Periodontal Health, Cytokine Levels, and Immunoglobulins. Biomed Res. Int. 2022 Apr 23;2022:6476597. doi: 10.1155/2022/6476597. PMID: 35502340; PMCID: PMC9056215.

17. Lee DH, Kim NR, Lim B-S, Lee Y-K, Yang H-C. Effects of TEGDMA and HEMA on the expression of COX-2 and iNOS in cultured murine macrophage cells. Dent Mater. 2009; 25:240-6.

18. De Nys S, Duca RC, Vervliet P, Covaci A, Boonen I, Elskens M, Vanoirbeek J, Godderis L, Van Meerbeek B, Van Landuyt KL. Bisphenol A as degradation product of monomers used in resin-based dental materials. Dent Mater. 2021; 37:1020-9.

19. Volk J, Engelmann J, Leyhausen G, Geurtsen W. Effects of three resin monomers on the cellular glutathione concentration of cultured human gingival fibroblasts. Dent Mater. 2006;22:499-505.

20. Eckhardt A, Gerstmayr N, Hiller KA, Bolay C, Waha C, Spagnuolo G, Camargo C, Schmalz G, Schweikl H. TEGDMA-induced oxidative DNA damage and activation of ATM and MAP kinases. Biomaterials 2009;30:2006-14.

21. Nocca G, De Palma F, Minucci A, De Sole P, Martorana GE, Callà C, Morlacchi C, Gozzo ML, Gambarini G, Chimenti C. Alterations of energy metabolism and glutathione levels of HL-60 cells induced by methacrylates present in composite resins. J Dent. 2007;35:187-94.

22. Schweikl H, Spagnuolo G, Schmalz G. Genetic and cellular toxicology of dental resin monomers. J Dent Res. 2006;85:870-7.

23. Shehata M, Durner J, Eldenez A, Van Landuyt K, Styllou P, Rothmund L, Hickel R, Scherthan H, Geurtsen W, Kaina B. Cytotoxicity and induction of DNA double-strand breaks by components leached from dental composites in primary human gingival fibroblasts. Dent Mater. 2013;29:971-9.

24. Koulaouzidou EA, Roussou K, Sidiropoulos K, Nikolaidis A, Kolokuris I, Tsakalof A, Tsitsimpikou C, Kouretas D. Investigation of the chemical profile and cytotoxicity evaluation of organic components eluted from pit and fissure sealants. Food Chem Toxicol. 2018;120:536-43.

25. Susila AV, Balasubramanian V. Correlation of elution and sensitivity of cell lines to dental composites. Dent Mater. 2016;32:e63-72.

26. Krifka S, Seidenader C, Hiller KA, Schmalz G, Schweikl H. Oxidative stress and cytotoxicity generated by dental composites in human pulp cells. Clin Oral Investig. 2012;16:215-24.

27. Kashiwagi K, Inoue H, Komasa R, Hosoyama Y, Yamashita K, Morisaki A, Goda S. Optimal dilutions of S-PRG filler eluate for experiments on human gingival fibroblasts in vitro. Dent Mater J. 2021;40:136-42.

28. Reidelbach C, Garcia-Käufer M, Wingert N, Arif A, Vach K, Hellwig E, Gminski R, Polydorou O. Cytotoxicity and estrogenicity in simulated dental wastewater after grinding of resin-based materials. Dent Mater. 2021;37:1486-97.

29. De Angelis F, Sarteur N, Buonvivere M, Vadini M, Šteffl M, D'Arcangelo C. Meta-analytical analysis on components released from resin-based dental materials. Clin Oral Investig. 2022 Jul 23. doi: 10.1007/s00784-022-04625-4. Epub ahead of print. PMID: 35870020.

30. Spahl W, Budzikiewicz H, Geurtsen W. Determination of leachable components from four commercial dental composites by gas and liquid chromatography/mass spectrometry. J Dent. 1998;26:137-45.

31. Di Francescantonio M, Pacheco RR, Aguiar TR, Boaro LCC, Braga RR, Martins AL, Giannini M. Evaluation of composition and morphology of filler particles in low-shrinkage and conventional composite resins carried out by means of SEM and EDX. J Clin Dent Res. 2016;13:49-58.

32. Delvallée A, Feltin N, Ducourtieux S, Trabelsi M. Comparison of nanoparticle diameter measurements by atomic force microscopy and scanning electron microscopy. In: 16th International Congress of Metrology. EDP Sciences. 2013.

33. Cebe MA, Cebe F, Cengiz MF, Cetin AR, Arpag OF, Ozturk B. Elution of monomer from different bulk fill dental composite resins. Dent Mater. 2015;31:e141-9.

34. Reichl FX, Seiss M, Marquardt W, Kleinsasser N, Schweikl H, Kehe K, Hickel R. Toxicity potentiation by H2O2 with components of dental restorative materials on human oral cells. Arch Toxicol. 2008; 82:21-8.

35. Michelsen VB, Moe G, Skålevik R, Jensen E, Lygre H. Quantification of organic eluates from polymerized resin-based dental restorative materials by use of GC/MS. J Chromatogr B. 2007;850:83-91.

36. Reichl FX, Löhle J, Seiss M, Furche S, Shehata MM, Hickel R, Müller M, Dränert M, Durner J. Elution of TEGDMA and HEMA from polymerized resin-based bonding systems. Dent Mater. 2012;28:1120-5.

37. Wei Su L, Lin DJ, Yen Uan J. Novel dental resin composites containing LiAl-F layered double hydroxide (LDH) filler: Fluoride release/recharge,

mechanical properties, color change, and cytotoxicity. Dent Mater. 2019;35:663-72.

38. Zheng L, Li K, Ning C, Sun J. Study on antibacterial and fluoride-releasing properties of a novel composite resin with fluorine-doped nano-zirconia fillers. J Dent. 2021;113:103772.

39. Putzeys E, Cokic SM, Chong H, Smet M, Vanoirbeek J, Godderis L, et al. Simultaneous analysis of bisphenol A based compounds and other monomers leaching from resin-based dental materials by UHPLC–MS/MS. J Sep Sci. 2017;40:1063-75.

40. Boaro LC, Lopes DP, de Souza AS, Nakano EL, Perez MD, Pfeifer CS, et al. Clinical performance and chemical-physical properties of bulk fill composites resin—a systematic review and meta-analysis. Dent Mater. 2019;35:e249-64.

41. Rinastiti M, Özcan M, Siswomihardjo W, Busscher HJ. Effects of surface conditioning on repair bond strengths of non-aged and aged microhybrid, nanohybrid, and nanofilled composite resins. Clin Oral Investig. 2011;15:625-33.

국 문 초 록

치과용 나노하이브리드 복합레진의 화학적 특성과 생체적합성에 관한 연구

JIANG ENSHI

치의과학과 치과생체재료과학

서울대학교 치의학대학원

목 적

본 연구에서는 나노하이브리드 복합레진의 필러 파티클 입자 크기 분포, 중합률, 반투명도를 측정하여 기본적 특징을 연구하고자 한다. 또한 복합레진의 용출물을 기체크로마토그래피 분석을 통하여 용출된 레진의 성분을 확인하고 용출물을 치은상피세포주에 적용한 뒤 세포독성, 실시간 세포내 활성산소의 축적, 세포의 증식 실험을 통하여 화학적특성과 생체적합성에 대해 연구하고자 한다.

방 법

세가지 나노하이브리드 복합레진(Tetric N-Ceram: TN; Ceram X Sphere Tec One: CX; and DenFil NX: DN) 을 선정하여 실험을 진행하였다. 나노하이브리드 복합레진의 필러 입자 크기의 분포를

확인하기 위해 전자현미경으로 촬영후 이미지 분석을 진행하였다(n = 5). 레진의 중합률을 측정하기 위해 광중합 진행(20 초, 40 초) 전후 마이크로 라만 스펙트로미터 장비로 측정 후 비교 분석하였다(n = 3). 반투명도 값은 복합레진을 10,000번 냉온 순환 자극 전후 측정하였다(n = 5). 광중합 후 복합레진의 용출물에 유리된 레진 성분을 확인하기 위해 기체크로마토그래피 질량분석을 진행하였다(n = 3). 치은섬유아세포주의 세포배양액은 복합레진을 용출하는데 사용되였고 복합레진은 24 시간 동안 용출하였다. 복합레진의 용출액을 사람의 치은 섬유아세포주에 적용하였으며 세포독성은 세가지 실험방법(WST-1, trypan blue exclusion, and live and dead assays)으로 진행하여 확인하였다(n =9). 실시간 세포내 활성산화 산소의 생성은 세포 이미지징 멀티모드 리더기 장비로 측정하였다(n =9). 그리고 7일 동안 복합레진의 용출물을 세포에 적용하여 세포증식에 주는 영향을 확인하였다(n =9). 통계분석은 ANOVA와 Bonferroni 사후분석법으로 통계적 유의성을 평가하였다(α = 0.05).

결 과

복합레진의 필러 입자의 형태와 크기의 분포는 서로 다르게 관찰되었으며 나노 필러의 함량은 TN 실험군에서 가장 적게, CX와 DN에서는 유사하게 측정되었다. 세가지 복합레진의 중할률에는 유의한 차이가 없었지만 40 초 광중합시 20 s 광중합 했을 때보다 유의하게 높았다($p < 0.05$). 냉온순화 자극 전후 세가지 복합레진의 반투명도 값에는 유의한 차이가 없었다($p > 0.05$). 기체크로마토그래피

정량분석시 서로 다른 구성의 단량체와 첨가제가 검출되였으며 CX 실험군의 triethylene glycoldimethacrylate (TEGDMA)의 양은 다른 두 실험군에 비해 높았다($p < 0.0001$). CX 실험군에서는 2-hydroxyethyl methacrylate(HEMA)가 검출되지 않았고 TN 실험군에서는 DN 실험군보다 높게 검출되였다($p = 0.0015$). BPA는 세가지 복합레진 모두 검출되지 않았다. 가장 높은 세포독성은 CX 실험군에서($p < 0.0001$), 가장 높은 세포활성은 DN 실험군에서 확인하였다($p < 0.0001$). 가장 높은 활성산화산소형성은 8, 12, 16시간째 모두 TN, CX, DN 실험군 순서로 측정되였다($p < 0.0001$). CX 실험군은 세포증식을 억제하였지만($p < 0.0001$) TN과 DN실험군은 세포증식에 영향을 주지 않았으며 대조군 NC와 비교시 유의한 차이가 없었다($p > 0.05$).

결 론

세가지 나노하이브리드 복합레진에서 여러가지 필러입자 크기 그리고 용출물에서 레진 성분을 확인하였으며 이는 서로 다른 세포 독성, 활성산화산소의 축적, 세포증식의 억제를 일으킨다. CX 그리고 TN 실험군 순서로 활성산화수소의 축적으로 인한 세포독성을 보였다. DN 실험군은 유의하게 높은 활성산화수소를 축적하지 않을 뿐더러 가장 높은 세포 활성을 보여주었다.

주요어: 나노하이브리드 컴포짓 레진, 활성산소, 세포적합성, 가스크로마토그래피/질량 분석

학 번: 2020-31168

Tables

Table 1. Materials used in this study (based on manufacturer data)

Material Group	Type	Composition (Matrix)	Composition (Filler)	Filler Degree (vol%, wt%)	Manufacturer (LOT No.)
Tetric N Ceram (TN)	Nano-hybrid	Bis-GMA UDMA Bis-EMA TEGDMA	Barium aluminium glass (0.4 μm, 0.7 μm) Ytterbium trifluoride (0.2 μm) Mixed oxide (0.16 μm) Prepolymer	55–57, 76	Ivoclar Vivadent, Lichtenstein (Y50557)
Ceram X Sphere Tec One (CX)	Nano-hybrid	Bis–EMA TEGDMA	The Sphere TEC fillers (15 μm) Nonagglomerated barium glass fillers (0.6 μm), Ytterbium fluoride (0.6 μm) Methacrylic polysiloxane nanoparticles	59–61, 77–79	Dentsply Sirona, USA (2009000471)
DenFil NX (DN)	Nano-hybrid	Bis-GMA UDMA TEGDMA	Barium aluminosilicate (< 1μm) Fumed silica (0.04 μm)	76–78, 81	Vericom, Korea (NX1601A2)

Table 2. Mean and standard deviations of the color component

	Color Components	TN	CX	DN	*p*-values
White	L^*	62.91 ± 13.91	62.03 ± 0.73	59.79 ± 0.81	0.91
	a^*	-0.11 ± 0.08	-0.16 ± 0.08	1.34 ± 0.03	> 0.99
	b^*	10.17 ± 3.49	9.18 ± 0.61	7.37 ± 0.25	> 0.99
Black	L^*	53.68 ± 13.98	52.8 ± 0.31	50.39 ± 1.12	0.83
	a*	-2.68 ± 1.22	-2.67 ± 0.09	-0.86 ± 0.02	> 0.99
	b*	-2.68 ± 1.22	-0.3 ± 0.13	-0.32 ± 0.12	> 0.99

Table 3. Main components found in the resin composites identified by GC/MS

Composite resin					TN	CX	DN
Compound name	**Function**	**Molecular Formula**	**Molecular Weight**	**t_R (min)**	**Area%**	**Area%**	**Area%**
HEMA	Monomer	$C_6H_{10}O_3$	130.14	10.06	21.70 ± 0.30	_	4.46 ± 0.15
TEGDMA	Monomer	$C_{14}H_{22}O_6$	286.32	21.65	0.26 ± 0.10	48.87 ± 3.90	3.77 ± 0.39
CQ	Photoinitiator	$C_{10}H_{14}O_2$	166.22	14.73	4.36 ± 0.58	0.78 ± 0.12	4.47 ± 0.18
DMABEE	Co-initiator	$C_{11}H_{15}NO_2$	193.24	19.77	9.02 ± 1.65	12.93 ± 1.85	13.49 ± 0.21
Benzyliodide	Others	C_7H_7I	218.03	12.55	_	3.81 ± 0.77	_
BHT	Inhibitor	$C_{15}H_{24}O$	220.35	17.23	_	8.82 ± 2.64	3.69 ± 1.61
Trans-1-Methyl-2-(4-methylpentyl)cyclopentane	Others	$C_{12}H_{24}$	168.32	17.58	11.68 ± 0.27	_	4.14 ± 0.31
HMBP	UV-absorber	$C_{14}H_{12}O_3$	228.24	23.22	_	2.02 ± 0.39	_
TINP	UV-stabilizer	$C_{13}H_{11}N_3O$	225.25	23.64	1.71 ± 0.21	_	1.49 ± 0.11
2-(3'-Hydroxy-4'-methoxyphenyl)-5-methoxy-3-(3",4",5-trimethoxyphenyl) benzofuran-6-o	Cyclooxygenase -inhibitor	$C_{25}H_{24}O_8$	452.45	35.62	10.35 ± 1.55	15.85 ± 1.39	33.59 ± 1.08
4,4'-[5-(1,1-Dimethylethyl)-2-methoxy-1,3-phenylene] bisdibenzofuran	Others	$C_{35}H_{28}O_3$	496.59	41.74	3.61 ± 0.90	1.67 ± 0.15	5.89 ± 0.07
DCHP	Plasticizer	$C_{20}H_{26}O_4$	330.42	27.35	2.46 ± 0.18	_	_

Abbreviation

HEMA: 2-Hydroxyethyl methacrylate

TEGDMA: Triethylene glycol dimethacrylate

CQ: Camphorquinone

DMABEE: 4-dimethyl amino benzoic acid ethyl ester

BHT: Butylatedhydroxytolune

HMBP: 2-Hydroxy-4-methoxybenzophenone

TINP: 2-(2-Hydroxy-5-methylphenyl) benzotriazole

DCHP: Dicyclohexyl Phthakate

Table 4. Standard components used in this study

Component	Cat. No.	Purity, wt-%	Manufacturer
UDMA	72869–86–4	≥ 97%	Sigma Aldrich
HEMA	868–77-9	≥ 97%	Sigma Aldrich
TEGDMA	109–16–0	≥ 97%	Sigma Aldrich
BPA	80–05–7	≥ 97%	Sigma Aldrich

Table 5. Quantification of substances in methanol eluates of three nanohybrid composite resin

Monomers (molecular weight)	**Mean ± SD amount components in the eluates of the composites µg/ml (mM)**			
	TN	CX	DN	P-values
HEMA (130.14)	259.46 ± 53.14[a] (1.99 ± 0.41)	–	43.91 ± 3.32[b] (0.34±0.02)	–
TEGDMA (286.32)	23.3 ± 0.06 [b] (0.08 ± 0.00)	1081.10 ± 128.60 [a] (3.77 ± 0.45)	38.80 ± 3.50 [b] (0.13 ± 0.12)	<0.0001
BPA (228.19)	–	–	–	–

Data are presented as the mean and standard error, and the different superscript lowercase letters indicate significant differences in columns (P <0.001)

Figures

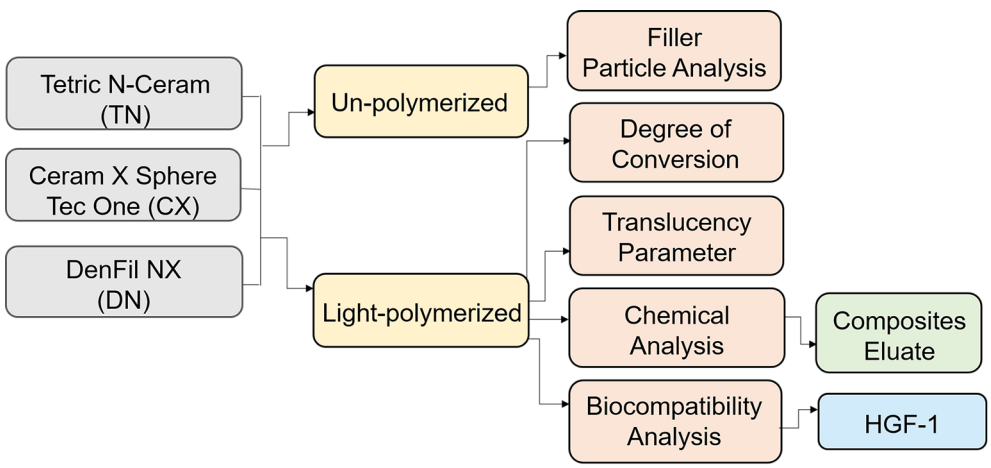

Figure 1. Experiment flow diagram

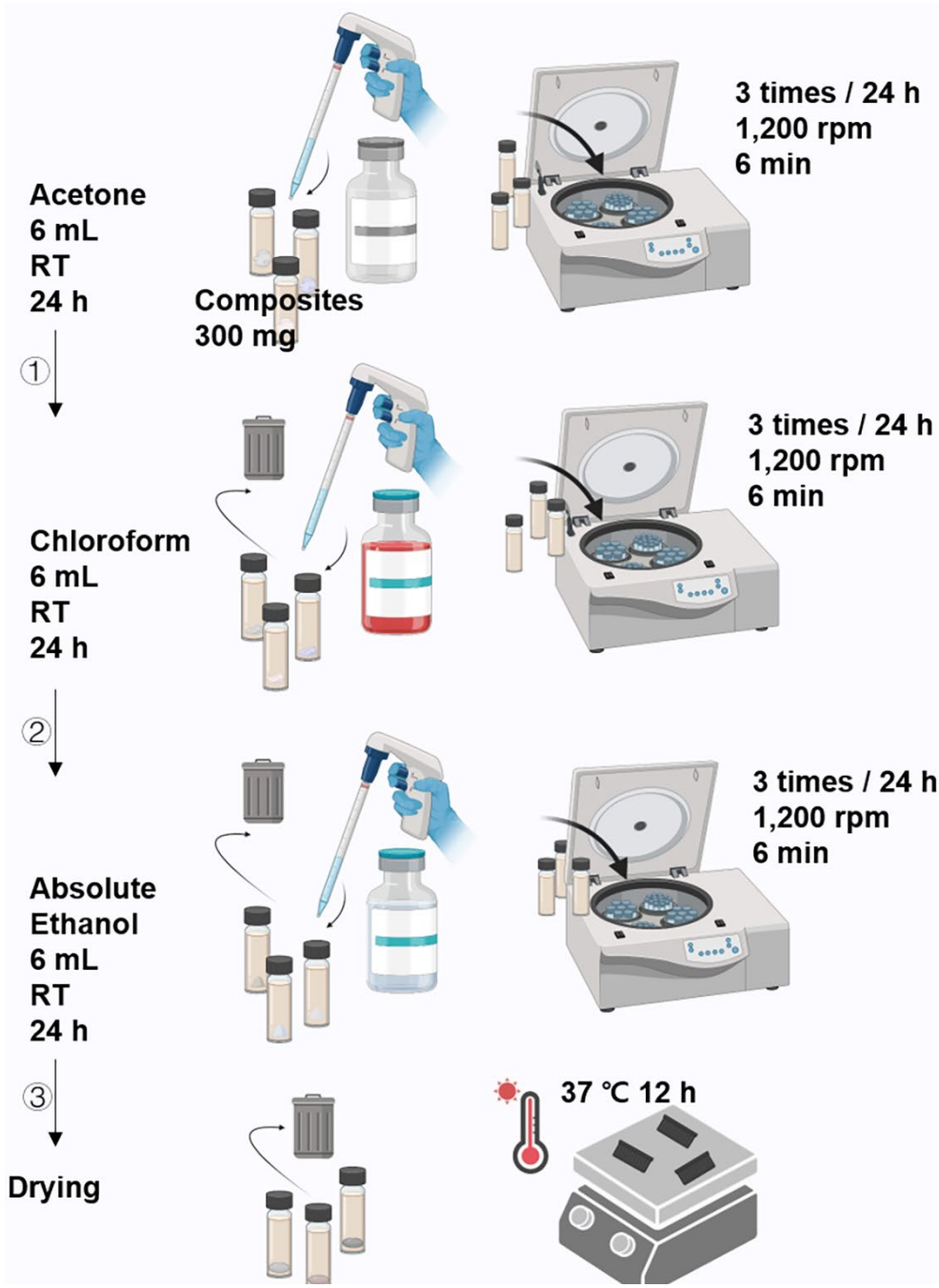

Figure 2. Filler particle preparation

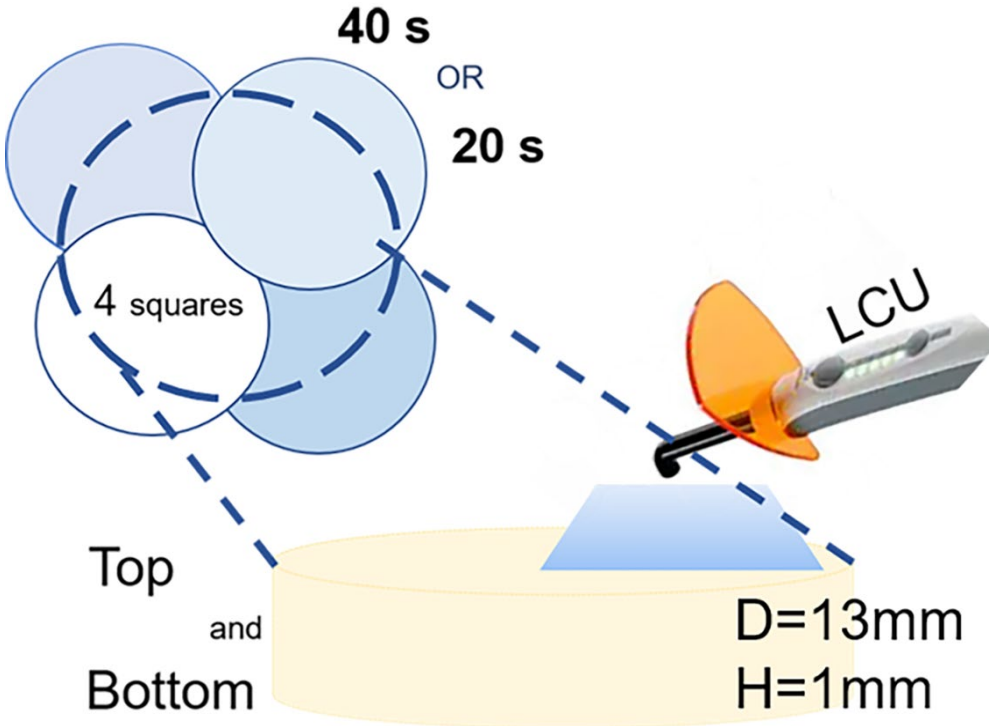

Figure 3. Light-polymerized specimen preparation

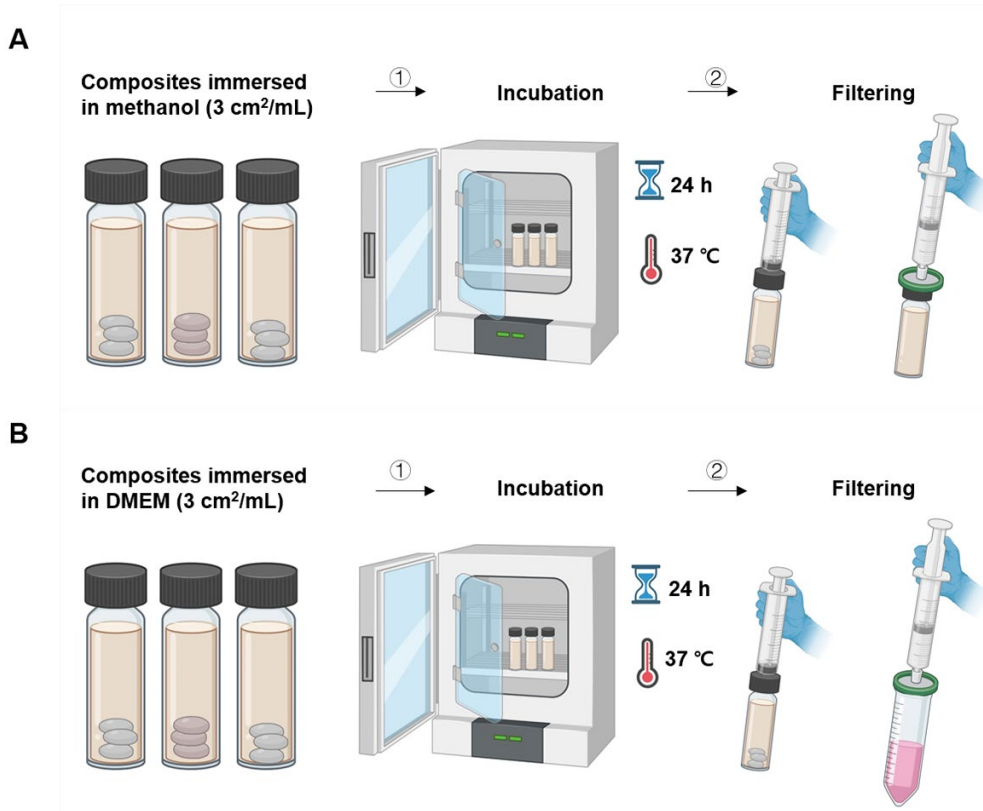

Figure 4. Composites eluate preparation (A) Light-polymerized composites eluted in methanol and composites eluate used in quantitative analysis. (B) Light-polymerized composites eluted in DMEM and composite eluate used in the biological test.

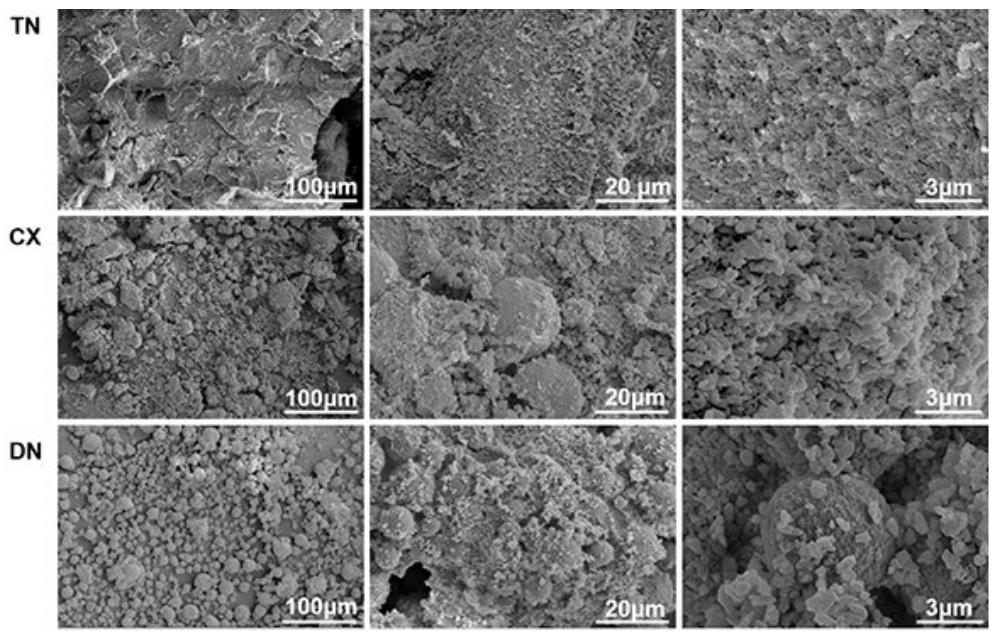

Figure 5. SEM images demonstrating the distribution of submicron-sized and spherical filler particles with their agglomeration features (magnification: left, 1,000×; center, 5,000×; right, 10,000×). Submicron-sized nanofillers aggregated to large spherical-shaped fillers were dominant in CX) and DN.

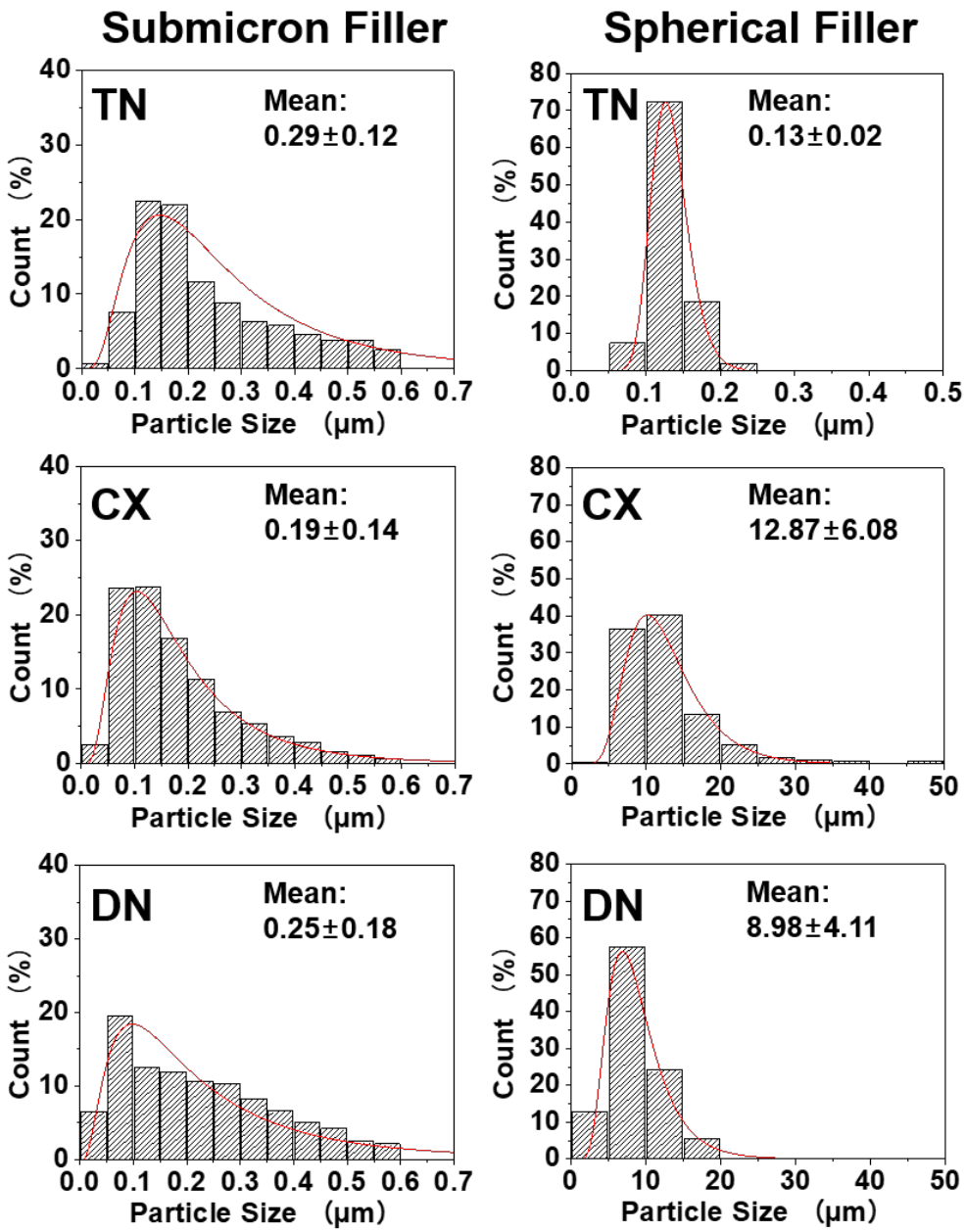

Figure 6. Distribution and the mean sizes of submicron and spherical filler particles in TN, CX, and DN.

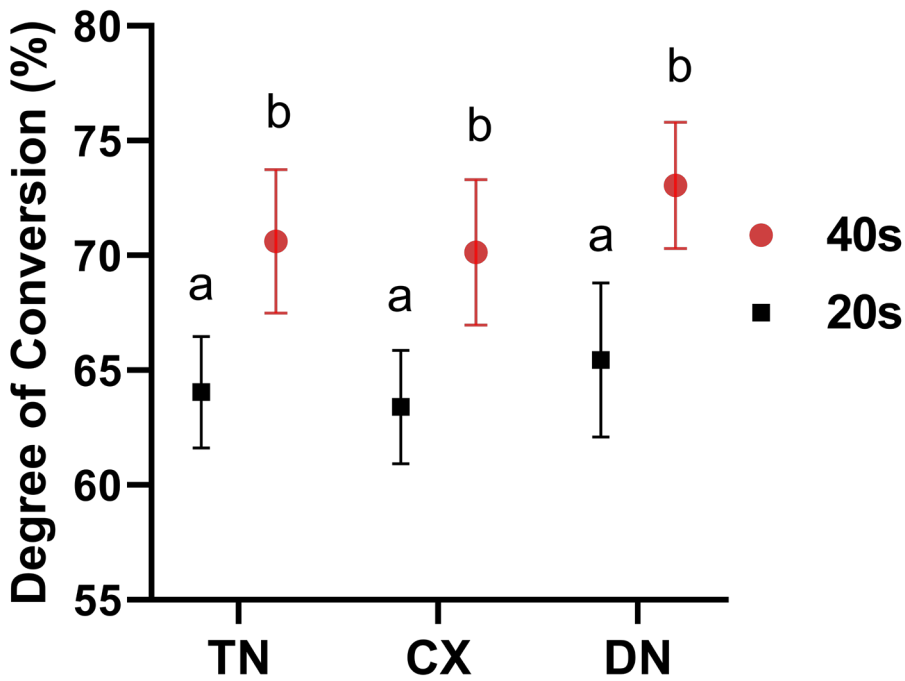

Figure 7. Mean values of the DC (standard deviation shown in error bars). Different letters represent statistically significant differences between the groups. There were no significant differences among the three composites. The DC of 40 s light-polymerized specimen was higher than that in 20 s ($p < 0.05$).

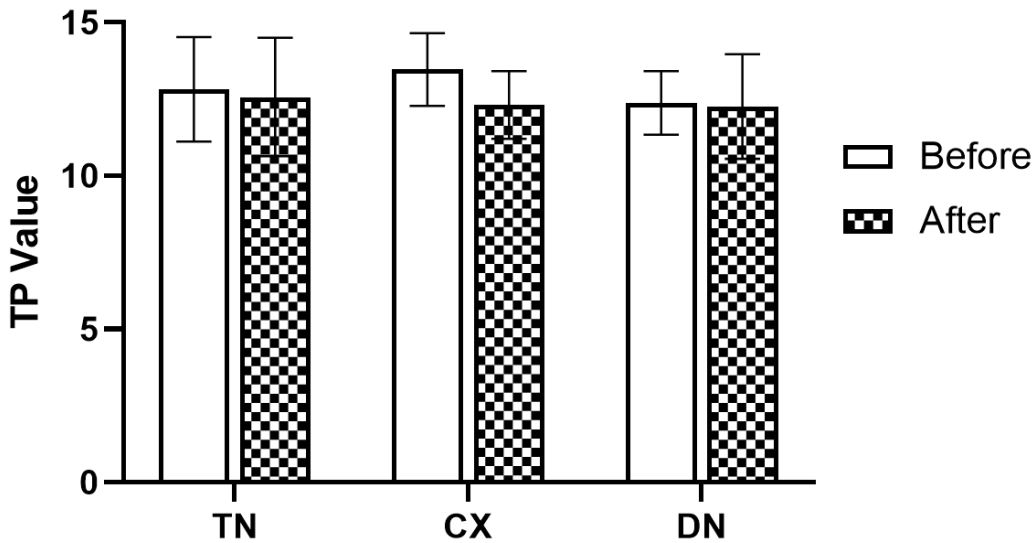

\

Figure 8. Mean TP values before and after thermocycling 1,000 times (standard deviation shown in error bars). There were no significant differences among the three composites ($p > 0.05$).

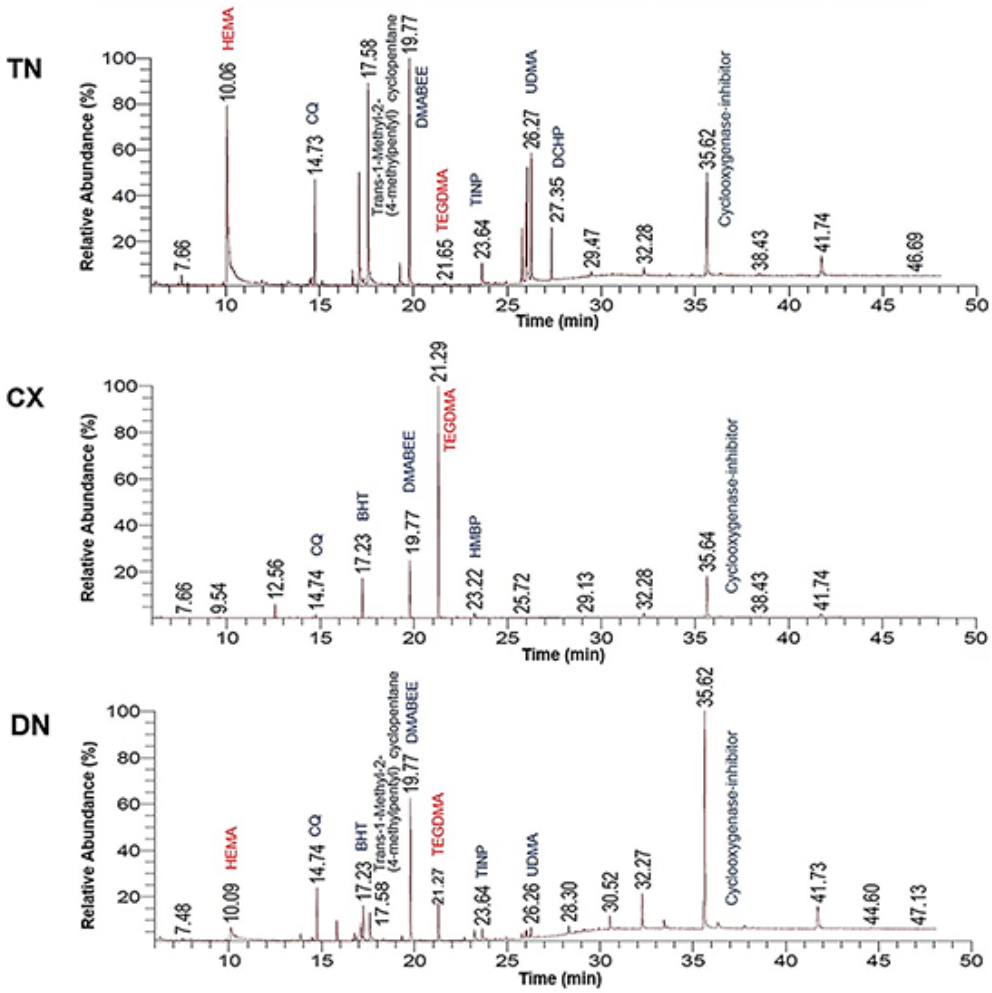

Figure 9. GC/MS chromatogram demonstrates different compositions of monomers and additives in TN, CX, and DN. The percentages of an area refer to the total area of the peaks from the retention time of 0 to 50 min.

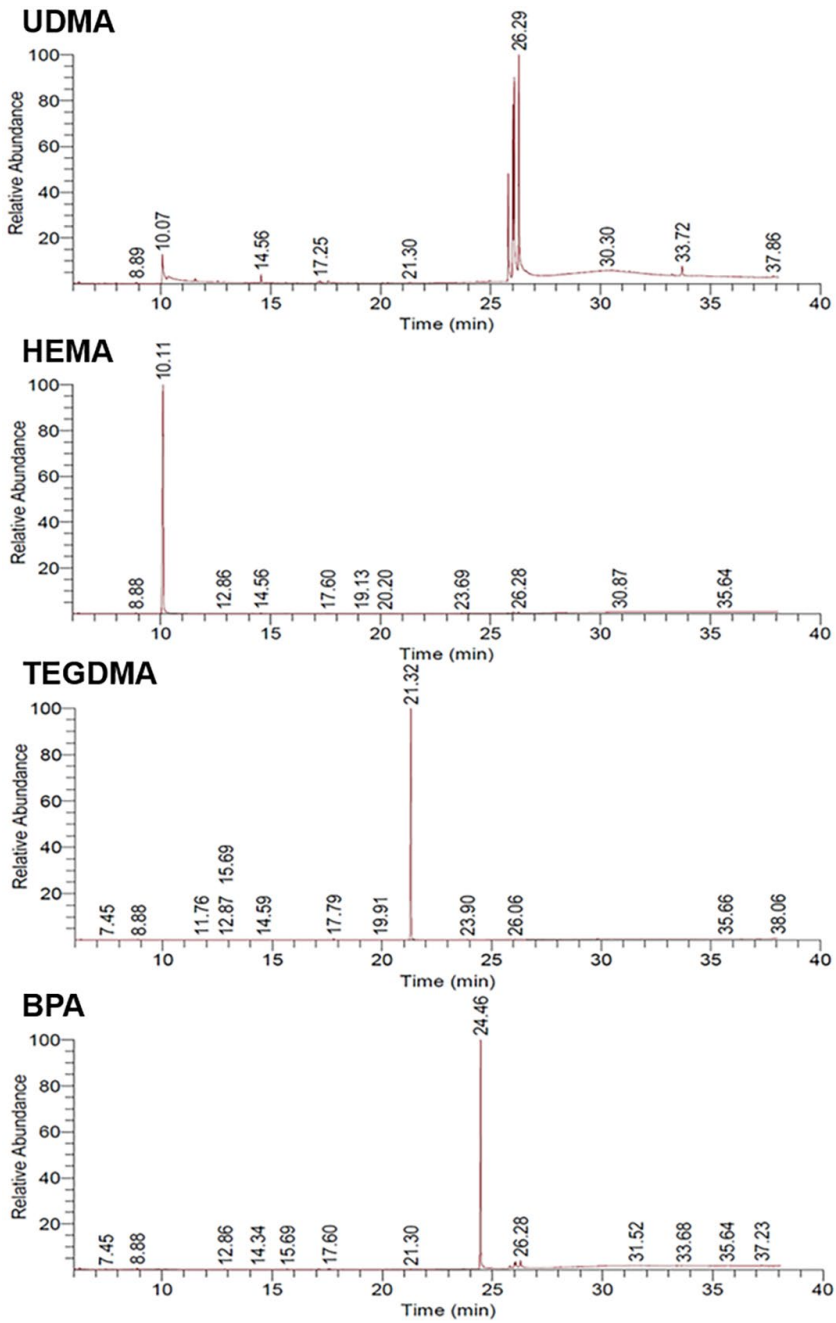

Figure 10. Standard component detection. GC/MS analysis of UDMA was characterized by four single peaks at 26.29 min and a single peak of 2-hydroxyethyl methacrylate (HEMA) at 10.07 min. GC/MS analysis of HEMA, TEGDMA, and BPA releaved single peaks at 10.11 min, 21.32 min, and 24.46 min, respectively.

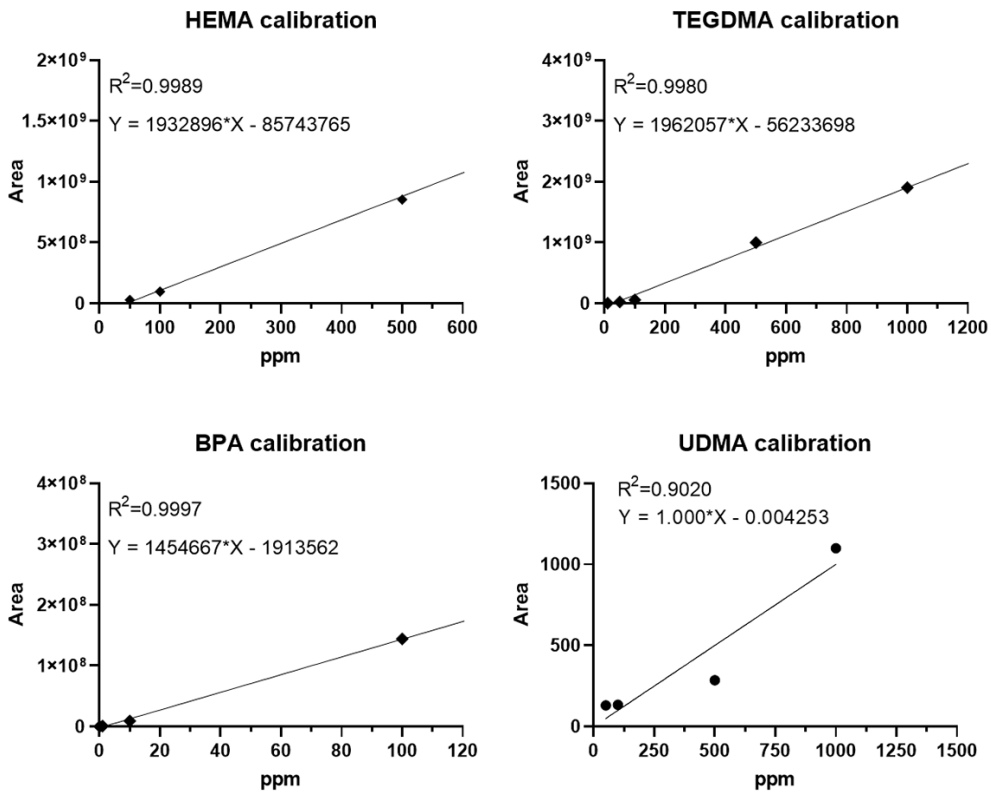

Figure 11. Calibration curves for standard components (TEGDMA, HEMA, BPA, and UDMA).

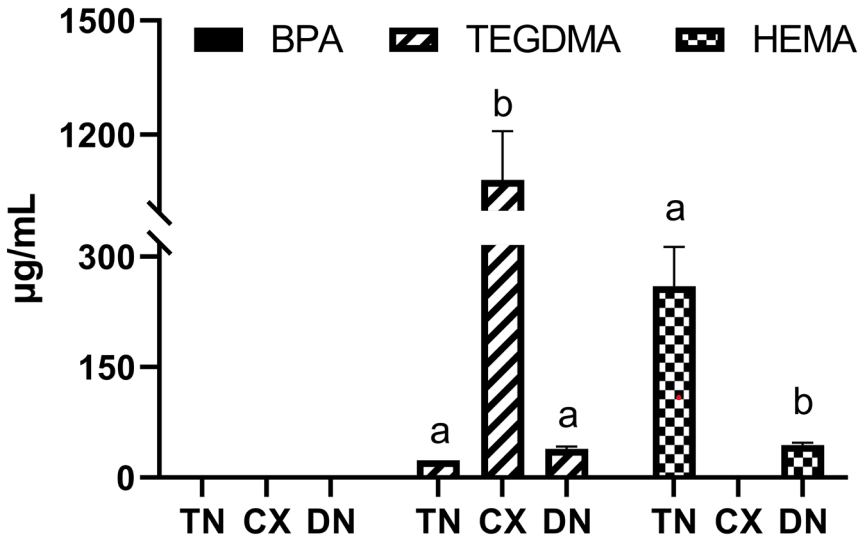

Figure 12. Quantification of substances in methanol eluates of three nanohybrid composite resins**.** Data are presented as the mean and standard error; the different letters represent statistically significant differences among groups ($p < 0.0001$). BPA was not detected in three composite eluates. TEGDMA was highest in CX compared with TN and DN. HEMA was higher in TN compared with DN, while no HEMA was detected in CX.

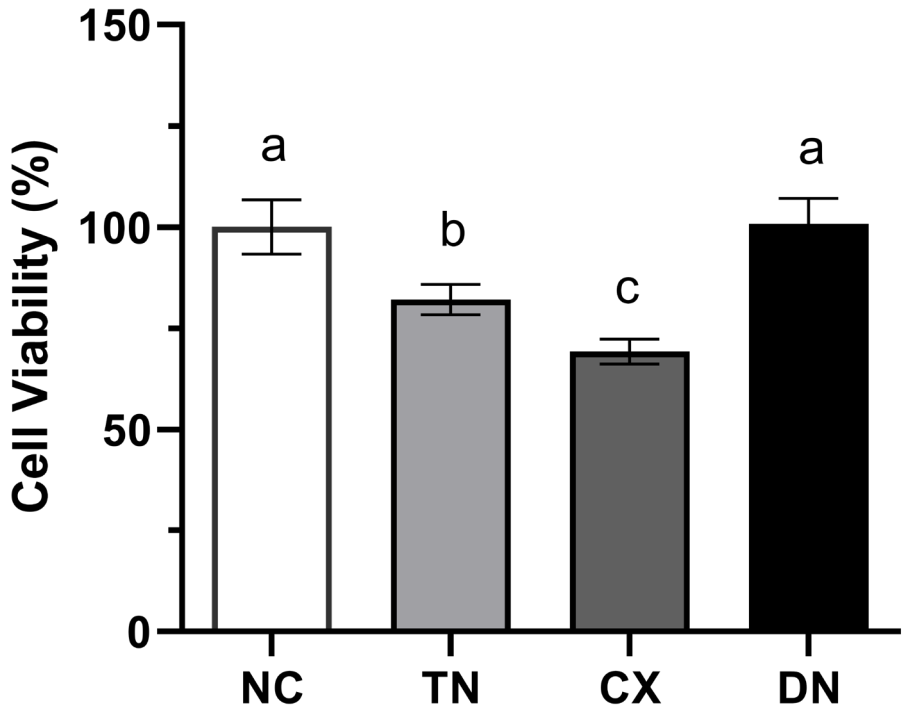

Figure 13. Relative cell viability of HGF-1 cells exposed to NC (cell culture medium) and three composites (TN, CX, and DN) eluate. Data are presented as the mean and standard error; different letters represent statistically significant differences among groups ($p < 0.0001$). There was a significant difference in TN and CX compared with NC.

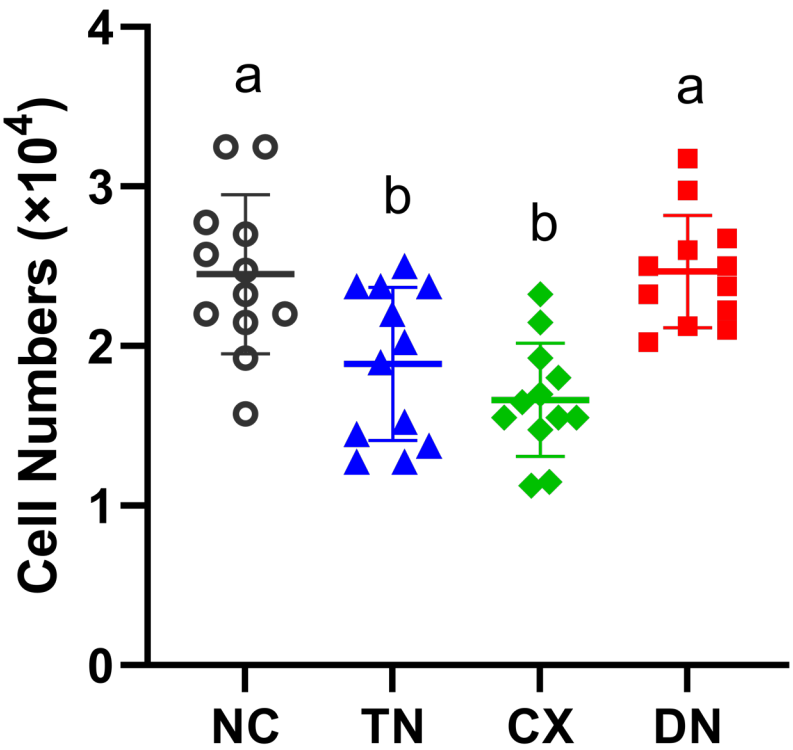

Figure 14. HGF-1 cell numbers after exposure to NC and three composite eluates (TN, CX, and DN). Data are presented as the mean and standard error; different letters represent statistically significant differences among groups ($p < 0.0001$). There was a significant difference in TN and CX compared with NC.

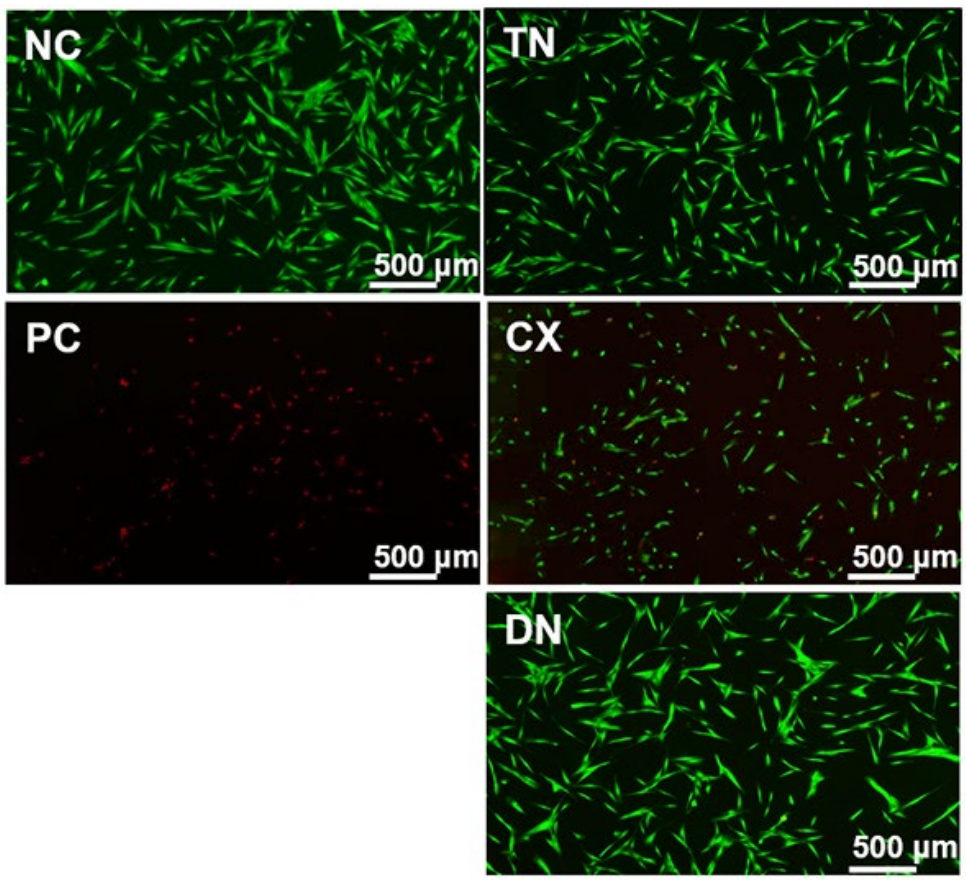

Figure 15. Representative images of HGF-1 treated with eluates from TN, CX, and DN in live/dead assays, compared to NC and PC (positive control) treated with 1 mM H_2O_2. Merged fluorescent images with viable cells appear in green and dead cells in red. Dead cells were dominant in PC and changes in cell morphology are shown in CX. The majority of viable cells and rare dead cells in TN, DN, and NC are shown.

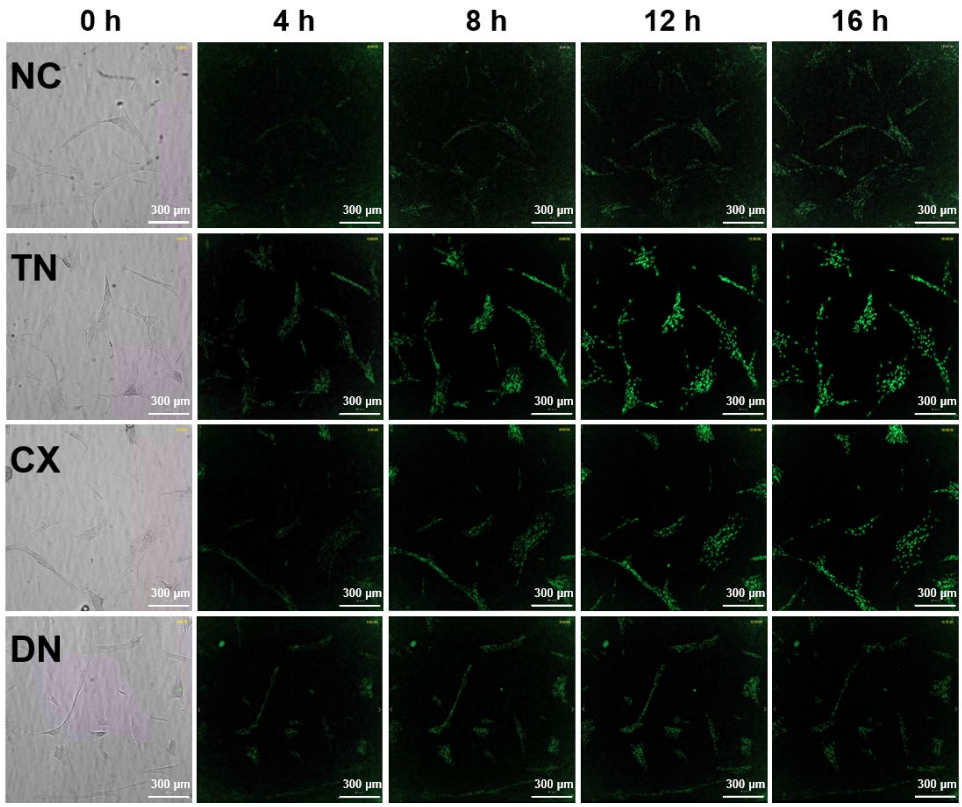

Figure 16. Real-time ROS detection images via fluorescent staining of HGF-1 cells treated with composite eluates. Green fluorescence is more evident in TN and CX compared to NC. TN and CX showed increased fluorescence signals from 8 h to 16 h. NC and DN showed no fluorescence signals for 16 h.

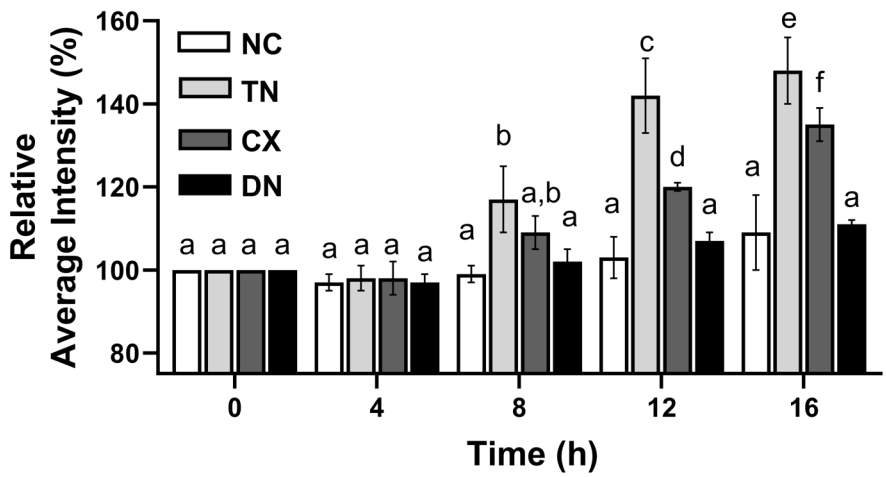

Figure 17. The GFP intensity percentages of every 4h. Data are presented as the mean and standard error, and the different letters represent statistically significant differences among the group ($p < 0.0001$). TN and CX showed a significantly higher intensity at 8, 12, and 16 h compared with NC.

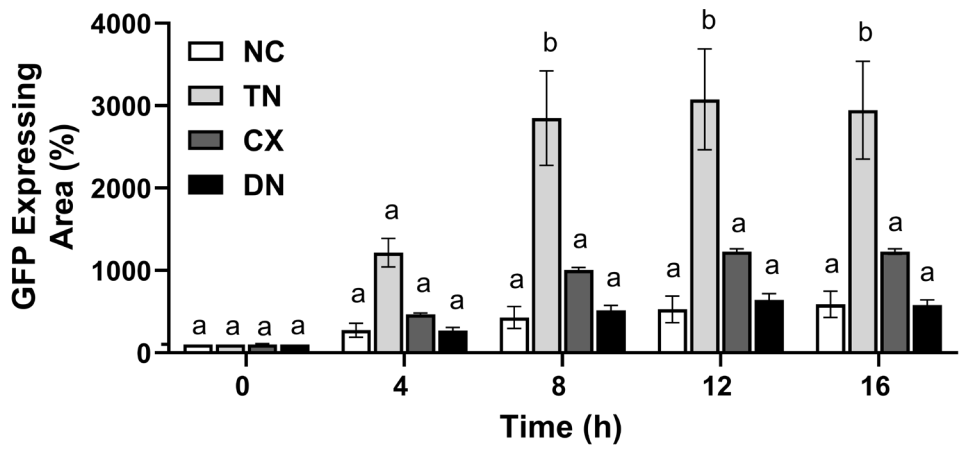

Figure 18. The GFP expression area percentage of every 4 h. Data are presented as the mean and standard error, and the different letters represent statistically significant differences among the group ($p < 0.0001$). TN significantly increased at 8, 12, and 16 h compared with NC.

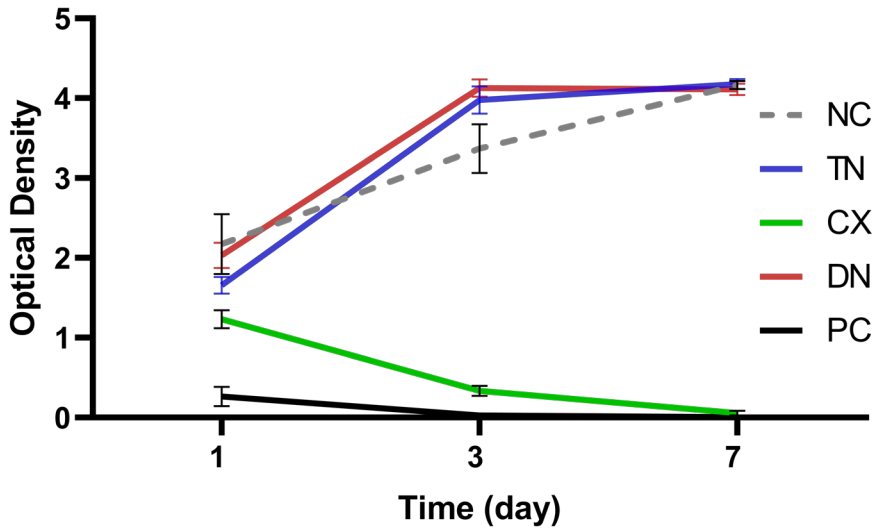

Figure 19. The OD of each group at 1, 3, and 7 days are presented as the means and standard deviation. OD values decreased in CX and PC, but increased in NC, TN, and DN

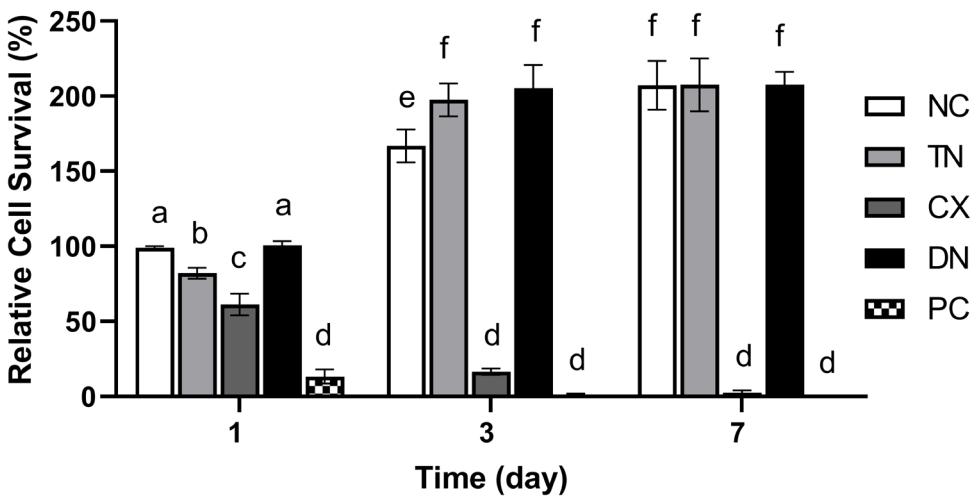

Figure 20. Relative cell survival of each group at 1, 3, and 7 days. Data are presented as the mean and standard error; different letters represent statistically significant differences among groups ($p < 0.0001$). Relative cell survival of CX was lower than that of NC, TN, and DN on 1, 3, and 7 days. Relative cell survival of TN and DN was higher than that of NC on day 3.